Divergence-type 2 + 1 dissipative hydrodynamics applied to heavy-ion collisions

J. Peralta-Ramos* and E. Calzetta†

Departamento de Física, FCEyN, Universidad de Buenos Aires and Instituto de Física de Buenos Aires, CONICET Ciudad Universitaria, Pabellón I, 1428 Buenos Aires, Argentina

(Received 7 March 2010; revised manuscript received 18 October 2010; published 15 November 2010)

We apply divergence-type theory (DTT) dissipative hydrodynamics to study the 2 + 1 space-time evolution of the fireball created in Au+Au relativistic heavy-ion collisions at $\sqrt{s_{NN}} = 200$ GeV. DTTs are exact hydrodynamic theories that do not rely on velocity gradient expansions and therefore go beyond second-order theories. We numerically solve the equations of motion of the DTT for Glauber initial conditions and compare the results with those of second-order theory based on conformal invariance (Baier-Romatschke-Son-Starinets model) and with data. We find that the charged-hadron minimum-bias elliptic flow reaches its maximum value at lower p_T in the DTT, and that the DTT allows for a value of η/s slightly larger than that of the BRSS. Our results show that the differences between viscous hydrodynamic formalisms are a significant source of uncertainty in the precise extraction of η/s from experiments.

DOI: 10.1103/PhysRevC.82.054905 PACS number(s): 12.38.Mh, 25.75.Ld, 47.10.A−, 47.75.+f

I. INTRODUCTION

The heavy-ion collision experiments performed at BNL's Relativistic Heavy Ion Collider (RHIC) create a hot and dense medium, the quark-gluon plasma (QGP). One of the most important discoveries at RHIC is the large elliptic flow in noncentral Au+Au collisions, which is a clear indication of collective behavior. By now, it is generally agreed that the QGP thermalizes on times $\lesssim$2.5 fm/c and behaves as a fluid with one of the lowest viscosity-to-entropy ratios observed in nature, $\eta/s \lesssim 0.5$ [1–3].

In recent years, relativistic hydrodynamics has become an efficient tool for describing the evolution of the fireball created at RHIC (there is a vast literature on this subject; see, for instance, Refs. [1,4–15]). Ideal hydrodynamics has been partly successful in explaining the observed collective flow at low transverse momentum and in central collisions [16]. Nevertheless, one should notice that when using a realistic equation of state (including a crossover phase transition) and allowing for separate kinetic and chemical freeze-outs, it seems difficult to fit the data with ideal hydrodynamics [1,17–21]. Moreover, if one aims eventually to derive the QGP viscosity from experimental data, one must start from a theoretical framework that allows for such effects.

When one attempts to formulate a relativistic real hydrodynamics one finds that there is simply no equivalent to the nonrelativistic Navier-Stokes equations. A straightforward relativistic generalization of the Navier-Stokes equations yields the so-called first-order theories. These theories are plagued with causality and stability problems [6,15,22]. One is therefore led to consider the so-called second-order theories (SOTs). These theories are presented as an expansion of the viscous tensor in velocity gradients, neglecting all orders higher than the second. They are unreliable in situations where these gradients are strong, and indeed they are known to fail, for example, in the description of strong shocks [23,24]. It is then valuable to develop alternative theories, not limited to weak velocity gradients, to provide at least an estimate of the expected accuracy of the gradient expansion.

With this in mind, in Ref. [25] the present authors developed a hydrodynamical description of a conformal field within the framework of the so-called divergence-type theories (DTTs) developed by Geroch [26] (see also Refs. [27–29]). DTTs do not rely on velocity gradient expansions and, in this sense, they go beyond second-order theories. The purpose of this work is to present numerical results obtained from solving the equations of the DTT in 2 + 1 dimensions. We use the equations to simulate Au+Au collisions, and compare the results both to experimental data and to a representative SOT. As was done in previous studies by other groups, we limit ourselves to boost-invariant longitudinal expansion in flat space-time.

In past years, there have been numerous theoretical studies of viscous hydrodynamics in 2 + 1 dimensions applied to heavy-ion collisions [9,11,20,21,30–33]. Most previous works employ Israel-Stewart formalism or some variation of it in order to simulate the evolution of the fireball. Very recently, Luzum and Romatschke [20,21] performed detailed simulations of Au+Au collisions based on the conformal hydrodynamical equations. The consistent picture that emerges from these diverse studies is that it is possible to match viscous hydrodynamics results to experimental data, provided $\eta/s \lesssim$ (5–6) $\times 1/(4\pi)$ [3,5,20,21]. See also [34,35].

In this paper we shall choose as the prototype SOT the one developed by Baier *et al.* [36] (see also Bhattacharyya *et al.* [37] and Natsuume *et al.* [38]). For simplicity we will refer to this hydrodynamic theory as BRSS (Baier-Romatschke-Son-Starinets). The BRSS theory is based on conformal invariance and extends the well-known Israel-Stewart (IS) formalism [22] in that it contains *all* second-order terms that can appear in the stress-energy tensor of a conformal fluid [6,39]. The reason to study conformal field hydrodynamics is that it is relevant to the QGP since, as shown by lattice calculations [40], QCD is approximately conformal at high temperatures. In addition, a wealth of information of the strongly interacting plasma

*jperalta@df.uba.ar
†calzetta@df.uba.ar

such as transport coefficients (inaccessible to kinetic theory) can be obtained from the anti–de Sitter conformal field theory correspondence [10,36–38].

The main results we arrive at are (i) the momentum anisotropy is smaller in the DTT than in the BRSS theory, (ii) the charged-hadron minimum-bias elliptic flow reaches its maximum value at lower p_T in the DTT, and (iii) the matching of DTT results to data allows a viscosity-to-entropy ratio slightly larger than that of the BRSS theory.

We should note here that in any hydrodynamic simulation there are numerous sources of uncertainty, such as those coming from the initial conditions, from the freeze-out procedure, and from hadron dynamics (just to mention a few), which unfortunately prevent a precise determination of η/s. Ours is not the exception, and here we merely intend to show that the DTT is an alternative to SOTs in the modeling of heavy-ion collisions (an alternative that may prove useful in those cases where large velocity gradients are present, e.g., shock waves [23]). The results we obtain also show that the differences between hydrodynamic formalisms are a significant source of uncertainty in the precise extraction of η/s from data. This indubitably points to the conclusion that, until these uncertainties are under control, care should be taken when attempting to extract η/s from hydrodynamic simulations. In this sense, the values for η/s presented in this work should be regarded as rough estimates.

This paper is organized as follows. In Sec. II we present the $2+1$ hydrodynamic equations of the BRSS and of the DTT, and describe the initial conditions, the equation of state (EOS), and the freeze-out prescription employed in the simulations. In Sec. III we present and discuss the results obtained, and in Sec. IV we present our conclusions. In Appendix A we evaluate the sensitivity of the results on the values of second-order transport coefficients and on the spatial mesh used in the simulations. In Appendix B we give a brief overview of divergence-type theories and derive Eq. (8).

II. THEORETICAL SETUP

A. Hydrodynamic equations

In this section we present the hydrodynamic equations of the BRSS theory and of the DTT for boost-invariant flow in $2+1$ dimensions. We employ Milne coordinates defined by proper time $\tau = \sqrt{t^2 - z^2}$ and rapidity $\psi = \operatorname{arctanh}(z/t)$, and, as mentioned in the Introduction, work in flat space-time. In these coordinates the metric tensor reads $g_{\mu\nu} = (1,-1,-1,-\tau^2)$. It is convenient to use Cartesian coordinates (x, y) in the transverse plane (instead of polar coordinates) since in this way the only nonvanishing Christoffel symbols are $\Gamma^{\tau}_{\psi\psi} = \tau$ and $\Gamma^{\psi}_{\tau\psi} = 1/\tau$. The fluid velocity is $\vec{u} = (u^\tau, u^x, u^y, 0)$ and is normalized as $u_\mu u^\mu = 1$.

The stress-energy tensor for dissipative relativistic hydrodynamics is

$$T^{\mu\nu} = \rho u^\mu u^\nu - p\Delta^{\mu\nu} + \Pi^{\mu\nu} \quad \text{with} \quad \Delta^{\mu\nu} = g^{\mu\nu} - u^\mu u^\nu, \tag{1}$$

where ρ and p are the energy density and the pressure in the local rest frame, and $\Pi^{\mu\nu}$ is the viscous shear tensor that is transverse ($u_\mu \Pi^{\mu\nu} = 0$), traceless, and symmetric. The tensor $\Delta^{\mu\nu}$ is the spatial projector orthogonal to u^μ. For a conformal fluid we have $T^\mu_\mu = 0$, so $\rho = 3p$ and the bulk viscosity vanishes.

In what follows, Latin indices stand for transverse coordinates (x, y), D^μ is the geometric covariant derivative, $D = u_\mu D^\mu$ and $\nabla^\mu = \Delta^{\mu\nu} D_\nu$ are the comoving time and space derivatives, respectively, and $\langle \cdots \rangle$ denotes the spatial, symmetric, and traceless projection of a tensor:

$$A^{\langle\mu\nu\rangle} = \left(\tfrac{1}{2}\Delta^{\mu\alpha}\Delta^{\gamma\nu} + \tfrac{1}{2}\Delta^{\mu\gamma}\Delta^{\alpha\nu} - \tfrac{1}{3}\Delta^{\mu\nu}\Delta^{\alpha\gamma}\right) A_{\alpha\gamma}. \tag{2}$$

The hydrodynamic equations are the conservation equations for the stress-energy tensor together with the evolution equation for the shear tensor $\Pi^{\mu\nu}$. The former reads

$$\begin{aligned} (\rho + p) Du^i &= \tfrac{1}{3}(g^{ij}\partial_j \rho - u^i u^\alpha \partial_\alpha \rho) - \Delta^i_\alpha D_\beta \Pi^{\alpha\beta}, \\ D\rho &= -(\rho + p)\nabla_\mu u^\mu + \Pi^{\mu\nu}\sigma_{\mu\nu}, \end{aligned} \tag{3}$$

where

$$\begin{aligned} D_\beta \Pi^{\alpha\beta} = {} & \Pi^{i\alpha}\partial_\tau \frac{u_i}{u_\tau} + \frac{u_i}{u_\tau}\partial_\tau \Pi^{i\alpha} + \partial_i \Pi^{i\alpha} \\ & + \Gamma^\alpha_{\beta\gamma}\Pi^{\beta\gamma} + \Gamma^\beta_{\beta\gamma}\Pi^{\alpha\gamma}. \end{aligned} \tag{4}$$

In the BRSS theory, the evolution of the shear tensor is given by [36]

$$\begin{aligned} \partial_\tau \Pi^{i\alpha} = {} & -\frac{4}{3u^\tau}\Pi^{i\alpha}\nabla_\mu u^\mu - \frac{1}{\tau_\pi u^\tau}\Pi^{i\alpha} + \frac{\eta}{\tau_\pi u^\tau}\sigma^{i\alpha} \\ & - \frac{\lambda_1}{2\tau_\pi \eta^2 u^\tau}\Pi^{\langle i}_\mu \Pi^{\alpha\rangle\mu} - \frac{u^i \Pi^\alpha_\mu + u^\alpha \Pi^i_\mu}{u^\tau} Du^\mu \\ & - \frac{u^j}{u^\tau}\partial_j \Pi^{i\alpha}, \end{aligned} \tag{5}$$

where η is the shear viscosity, (τ_π, λ_1) are second-order transport coefficients,

$$\sigma^{\mu\nu} = \nabla^{\langle\mu} u^{\nu\rangle} \tag{6}$$

is the first-order shear tensor, and

$$\begin{aligned} \nabla_\mu u^\mu &= \partial_\tau u^\tau + \partial_i u^i + \frac{u^\tau}{\tau}, \\ \nabla_{\langle x} u_{x\rangle} &= \Delta^{\tau x}\partial_\tau u^x + \Delta^{ix}\partial_i u^x - \tfrac{1}{3}\Delta^{xx}\nabla_\mu u^\mu, \\ \nabla_{\langle x} u_{y\rangle} &= \tfrac{1}{2}\Delta^{\tau x}\partial_\tau u^y + \tfrac{1}{2}\Delta^{\tau y}\partial_\tau u^x + \tfrac{1}{2}\Delta^{ix}\partial_i u^y \\ &\quad + \tfrac{1}{2}\Delta^{iy}\partial_i u^x - \tfrac{1}{3}\Delta^{xy}\nabla_\mu u^\mu, \\ \nabla_{\langle\psi} u_{\psi\rangle} &= \tau^4 \Delta^{\psi\psi}\Gamma^\psi_{\tau\psi} u^\tau - \tfrac{1}{3}\tau^4 \Delta^{\psi\psi}\nabla_\mu u^\mu. \end{aligned} \tag{7}$$

We note that in Eq. (5) we have neglected terms involving the fluid vorticity, which would be multiplied by additional second-order transport coefficients λ_2 and λ_3 [36,37]. The reason is that, for two-dimensional flow, it can be shown (see Refs. [20,21] and references therein) that if the vorticity is zero initially (as it is here), it will remain negligible throughout the evolution up to terms that are third order in velocity gradients (therefore, beyond the scope of second-order theory).

As already mentioned in the Introduction, the IS formalism is contained in the BRSS equations, as can be seen by setting $\lambda_1 = 0$.

In a DTT, the description of nonequilibrium hydrodynamic states requires the introduction of a new tensor $\xi^{\alpha\gamma}$, which is symmetric and traceless and vanishes in equilibrium [26]. For a conformal fluid, $\xi^{\alpha\gamma}$ must be transverse as well. The DTT provides an equation of motion for $\xi^{\alpha\gamma}$ (see Ref. [25] for details). For a conformal fluid in $2+1$ dimensions the evolution is given by

$$\begin{aligned}\partial_\tau \xi^{i\alpha} = &-\frac{2}{3u^\tau}\xi^{i\alpha}\nabla_\mu u^\mu - \frac{1}{\tau_\pi u^\tau}\xi^{i\alpha} + \frac{1}{\tau_\pi u^\tau}\sigma^{i\alpha} \\ &- \frac{\lambda_1}{3\tau_\pi \eta u^\tau}\xi_\mu^{\langle i}\xi^{\alpha\rangle\mu} - \frac{u^i\xi_\mu^\alpha + u^\alpha\xi_\mu^i}{u^\tau}Du^\mu \\ &- \frac{u^j}{u^\tau}\partial_j\xi^{i\alpha}. \end{aligned} \tag{8}$$

The shear tensor is calculated from the nonequilibrium tensor $\xi^{\alpha\gamma}$ as follows (see Appendix B):

$$\Pi^{\mu\nu} = \eta\xi^{\mu\nu} - \frac{\lambda_1\tau_\pi T^4}{3\eta}\left(\xi^{\mu\alpha}\xi_\alpha^\nu - \frac{1}{3}\Delta^{\mu\nu}\xi^{\alpha\gamma}\xi_{\alpha\gamma}\right). \tag{9}$$

The transport coefficients of the BRSS theory and the DTT are the same because the DTT goes over to BRSS at second order in velocity gradients. Note, however, that we are ignoring (possible) higher-order corrections to the transport coefficients of the DTT.

As independent variables we choose $(\rho, u^x, u^y, \Pi^{xx}, \Pi^{xy}, \Pi^{yy})$ for the BRSS and $(\rho, u^x, u^y, \xi^{xx}, \xi^{xy}, \xi^{yy})$ for the DTT. The τ component of the velocity follows from normalization, $u^\tau = \sqrt{1+u_x^2+u_y^2}$, while the other nontrivial components of $\Pi^{\mu\nu}$ (and of $\xi^{\mu\nu}$) follow from the transversality and tracelessness conditions.

In order to solve the hydrodynamic equations, we employ the method described in Ref. [41] (see also Ref. [20]). The set of six coupled differential equations is cast into a linear system for the time derivatives of the independent variables. This linear system is solved using a finite-difference method that is first-order accurate in the temporal grid spacing and second-order accurate in the spatial grid spacing. To be more precise, the derivatives are replaced by

$$\begin{aligned}\partial_\tau f(x,y,\tau) &= \frac{f(x,y,\tau+\delta\tau) - f(x,y,\tau)}{\delta\tau}, \\ \partial_x f(x,y,\tau) &= \frac{f(x+\delta x,y,\tau) - f(x-\delta x,y,\tau)}{2\delta x}\end{aligned} \tag{10}$$

and similarly for the derivative in y. We have made nontrivial tests on the code such as, for example, using uniform initial data in the $2+1$ numerical code to recover $(0+1)$-dimensional results (already presented in Ref. [25]).

B. Initial conditions and transport coefficients

Solution of the hydrodynamic equations requires initial conditions for the six independent variables. For the initial transverse velocity and shear tensor we use $u^x = u^y = 0$, which implies vanishing initial vorticity, and $(\Pi^{xx}, \Pi^{xy}, \Pi^{yy}) = 0$ or $(\xi^{xx}, \xi^{xy}, \xi^{yy}) = 0$. It has been shown in several works [20,21,30,31] that the evolution of the shear tensor $\Pi^{\mu\nu}$ is quite insensitive to the initialization values, the difference being appreciable only at very early times. We have verified that the elliptic flow shows very little sensitivity to the initialization of the shear tensor as well. In what follows, we take the initialization time to be $\tau_0 = 1$ fm/c.

The initial energy-density profile is calculated using a simple Glauber model [42], in which for impact parameter b we have

$$\rho(\tau_0, x, y, b) = C \times \sigma T_A\left(x + \frac{b}{2}, y\right) T_A\left(x - \frac{b}{2}, y\right), \tag{11}$$

where σ is 40 mb, C is a constant chosen such that $\rho(\tau_0, 0, 0, 0)$ corresponds to a given initialization temperature T_0 (via the equation of state), and T_A is the nuclear thickness function given by

$$T_A(x,y) = \int_{-\infty}^{\infty} \delta_A(x,y,z)\, dz. \tag{12}$$

The function δ_A is the Woods-Saxon density distribution for gold nuclei,

$$\delta_A(x,y,z) = \frac{\delta_0}{1 + \exp[(|\mathbf{x}| - R_0)/\chi]}, \tag{13}$$

with $\mathbf{x} = (x, y, z)$, $R_0 = 6.4$ fm, and $\chi = 0.54$ fm. The parameter δ_0 is chosen such that $\int d^3\mathbf{x}\delta_A(\mathbf{x}) = 197$ as appropriate for Au nuclei. We note that in all calculations we use a 7.5 fm $\times$ 7.5 fm transverse plane (we have used a 13 fm $\times$ 13 fm transverse plane and found that there is no significant change in our results).

Unless otherwise stated, we use values for the second-order transport coefficients corresponding to a strongly coupled $\mathcal{N} = 4$ super-Yang Mills (SYM) plasma [10,36–38]:

$$\tau_\pi = 2(2 - \ln 2)\frac{\eta}{sT} \quad \text{and} \quad \lambda_1 = \frac{\eta}{2\pi T}, \tag{14}$$

where s is the entropy density. We will show in Appendix A that our results depend only weakly on the precise value of second-order transport coefficients.

C. Equation of state

The set of hydrodynamic equations must be closed with an equation of state (EOS). Since we are interested in computing elliptic flow of the produced particles we must use an EOS including hadronization. We employ the EOS by Laine and Schröder [43] that connects a high-order weak-coupling perturbative QCD calculation at high temperatures to a hadron resonance gas at low temperatures, via an analytic crossover (as suggested by lattice QCD calculations [18,44]). We notice that this EOS is the same as that used in Ref. [20], so that the comparisons we make are meaningful (see also Ref. [18]).

D. Freeze-out

In order to compute the elliptic flow of produced particles, the freeze-out process must be simulated. To do so, we use the corresponding modules of the UVH2+1 code, which is described in detail in Refs. [20,21]. For completeness, we give here a brief overview of the Cooper-Frye freeze-out prescription [45] implemented in UVH2+1. For the isothermal freeze-out we use here, the conversion from hydrodynamic to particle degrees of freedom takes place in a three-dimensional hypersurface. The spectrum for a single on-shell particle with momentum $p^\mu = (E, \vec{p})$ and degeneracy d is

$$E\frac{dN}{d^3p} = \frac{d}{(2\pi)^3}\int p_\mu d\Sigma^\mu f(x^\mu, p^\mu), \tag{15}$$

where $d\Sigma^\mu$ is the normal vector on the hypersurface, and f is the *nonequilibrium* distribution function, customarily given by Grad's ansatz (see [15,20,21,39,46] for details)

$$\begin{aligned} f(x^\mu, p^\mu) &= f_0(x^\mu, p^\mu) + \delta f(x^\mu, p^\mu) = f_0(x^\mu, p^\mu) \\ &\quad + f_0(x^\mu, p^\mu)[1 \mp f_0(x^\mu, p^\mu)]\frac{p_\mu p_\nu \Pi^{\mu\nu}}{2T^2(p+\rho)} \\ &\simeq \exp\left(\frac{-p_\mu u^\mu}{T}\right)\left[1 + \frac{p_\mu p_\nu \Pi^{\mu\nu}}{2T^2(p+\rho)}\right]. \end{aligned} \tag{16}$$

The approximation in the second line holds when $p \gg T$, and it is used in our simulations. It has been shown in Refs. [20,21] that the systematic error of this approximation is very small at low transverse momentum $p_T \lesssim 2.5$ GeV, so we do not expect our results to have a significant error coming from this approximation.

The UVH2+1 freeze-out module calculates the spectra for particle resonances with masses up to 2 GeV and then determines the spectra of stable particles including feed-down contributions [47]. For this last step it uses the AZHYDRO package [48]. In this paper we will focus on the minimum-bias elliptic flow coefficient v_2 at central rapidity, which is given by

$$v_2(p_T) = \frac{\int dbb v_0(p_T, b)\tilde{v}_2(p_T, b)}{\int dbb v_0(p_T, b)}, \tag{17}$$

where the coefficients v_0 and $\tilde{v}_2$ are related to the particle spectra (including feed-down contributions) by

$$E\frac{dN}{d^3\vec{p}} = v_0(p_T, b)[1 + 2\tilde{v}_2(p_T, b)\cos(2\phi)], \tag{18}$$

where $\phi = \arctan(p_y/p_x)$ and $p_T = (p_x^2 + p_y^2)^{1/2}$. We note that kinetic and chemical freeze-out occur at the same temperature, which represents a simplification of the real process (see, for instance, Ref. [49] and references therein).

We may obtain an internal consistency check of the hydrodynamical approximation by computing elliptic flow (18) with the left-hand side given by Eq. (15) with the distribution function (16), or else with only the equilibrium distribution function. The difference between these two results is the so-called nonequilibrium contribution to elliptic flow δv_2.

It has been shown by Song and Heinz [31], by Chaudhuri [11,50], and by Dusling and Teaney [30] that, beyond $p_T \sim$ 2–3 GeV, the nonequilibrium correction to the momentum distribution function becomes comparable to the equilibrium contribution, thus rendering Grad's ansatz unreliable. A way to estimate the value of p_T at which this happens is to compare δv_2 to the total v_2. We note that this way of determining when Grad's ansatz becomes unreliable may miss corrections to the particle distribution function that are independent of azimuthal angle. However, it still provides an estimate that gives an idea of how large are the nonequilibrium corrections to the distribution function.

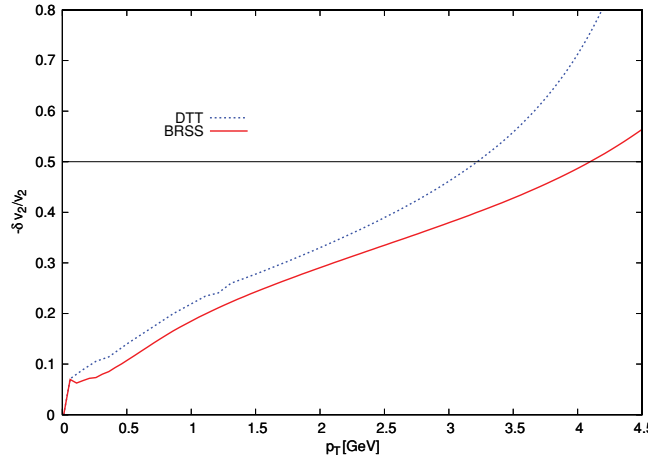

FIG. 1. (Color online) Nonequilibrium contribution to the total elliptic flow $-\delta v_2/v_2$ calculated with the BRSS and DTT with $\eta/s = 0.08$ and $b = 7$ fm. The initial and freeze-out temperatures are $T_i = 333$ MeV and $T_f = 140$ MeV in both models. The horizontal line indicates the (estimated) breakdown of Grad's ansatz.

In Fig. 1 we show $\delta v_2/v_2$ as a function of transverse momentum, calculated with the BRSS theory and the DTT with $\eta/s = 0.08$ and $b = 7$ fm. In this calculation, we set $T_i = 333$ MeV and $T_f = 140$ MeV in both models.

It is seen that, both in the BRSS theory and in the DTT, the nonequilibrium contribution to v_2 is significant even at low p_T. In the BRSS model δv_2 is always smaller than in the DTT, indicating that, in the latter, dissipative corrections to the nonequilibrium distribution function are larger. The difference between $\delta v_2/v_2$ calculated with the DTT and the BRSS grows with p_T, in particular, for $p_T > 3$ GeV, where $\delta v_2/v_2$ in the DTT starts growing faster. We can estimate the value of p_T at which Grad's ansatz becomes unreliable as that at which $-\delta v_2/v_2 \sim 0.5$, which is indicated by a horizontal line in the figure. In the DTT the value of p_T at which Grad's ansatz becomes unreliable turns out to be $p_T \sim 3.3$ GeV instead of $p_T = 4$ GeV as inferred in the BRSS model.

III. RESULTS

In this section we go over to our main goal in this paper, namely, to compare the results obtained with the DTT to RHIC data and to the BRSS results. We start by comparing the entropy production and the spatial and momentum anisotropies in both hydrodynamic models, and then proceed to compare particle multiplicity, $\langle p_T \rangle$, and elliptic flow to data in order to constrain the values of η/s.

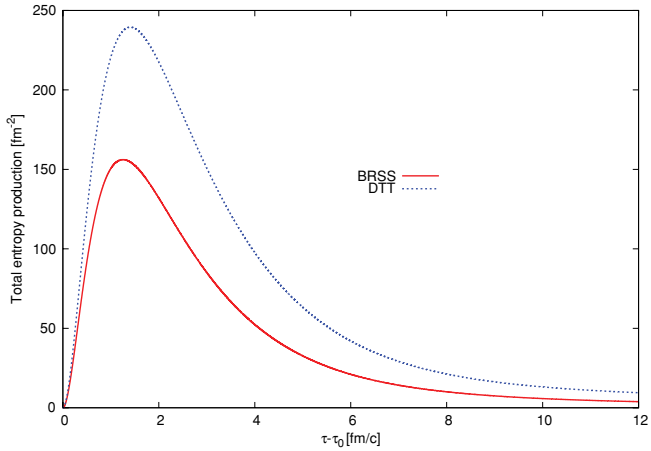

FIG. 2. (Color online) Total entropy production σ, given in Eq. (19), as a function of $\tau - \tau_0$ for the BRSS theory and the DTT with $\eta/s = 0.08$, $T_i = 333$ MeV, $T_f = 140$ MeV, and $b = 7$ fm.

Figure 2 shows the evolution of the total entropy production σ in a collision with impact parameter $b = 7$ fm, for the DTT and the BRSS with $\eta/s = 0.08$, an initial temperature $T_i = 333$ MeV, and a freeze-out temperature $T_f = 140$ MeV. The total entropy production is given by the following expressions:

$$\sigma_{\rm BRSS} \equiv \int dxdy(\partial_\mu S^\mu)|_{\rm BRSS} = \int dxdy \frac{\Pi^{\mu\nu}\Pi_{\mu\nu}}{2\eta T},$$
$$\sigma_{\rm DTT} \equiv \int dxdy(\partial_\mu S^\mu)|_{\rm DTT} = \int dxdy \frac{\eta\xi^{\mu\nu}\xi_{\mu\nu}}{2T}. \quad (19)$$

We note that in order for the comparison to make sense we have used the same T_i and η/s for the DTT and the BRSS model. It is seen that the entropy production is significantly larger in the DTT. At early (late) times the DTT produces ∼25% (∼40%) more entropy than the BRSS. However, at very early times $\tau - \tau_0 < 1$ fm/c the entropy production is the same in both models.

We now compare the spatial (ϵ_x) and momentum (ϵ_p) anisotropies, defined as

$$\epsilon_x = \frac{\langle y^2 - x^2\rangle_\rho}{\langle y^2 + x^2\rangle_\rho} \quad \text{and} \quad \epsilon_p = \frac{\langle T^{xx} - T^{yy}\rangle}{\langle T^{xx} + T^{yy}\rangle}, \quad (20)$$

where $\langle\cdots\rangle_\rho$ denotes an average procedure over the transverse plane with the energy density ρ as a weighting factor. In Fig. 3 we show ϵ_p calculated with the same value of $\eta/s = 0.08$, $T_i = 333$ MeV, and $T_f = 140$ MeV for the BRSS and the DTT. This allows us to determine the differences between both hydrodynamic formalisms. It is seen that ϵ_p is slightly smaller in the DTT, indicating that the DTT leads to larger shear stress and thus to larger dissipation. This is consistent with the fact that, as already discussed, more entropy is produced in the DTT.

We now allow the values of η/s to vary. In Fig. 4 we show the evolution of ϵ_x and ϵ_p for the BRSS and the DTT with $b = 7$ fm, $T_i = 333$ MeV, $T_f = 140$ MeV, and several values of η/s. The values of η/s correspond to those that will be suitable for matching kaon multiplicity and $\langle p_T\rangle$ to data, as will be shown later.

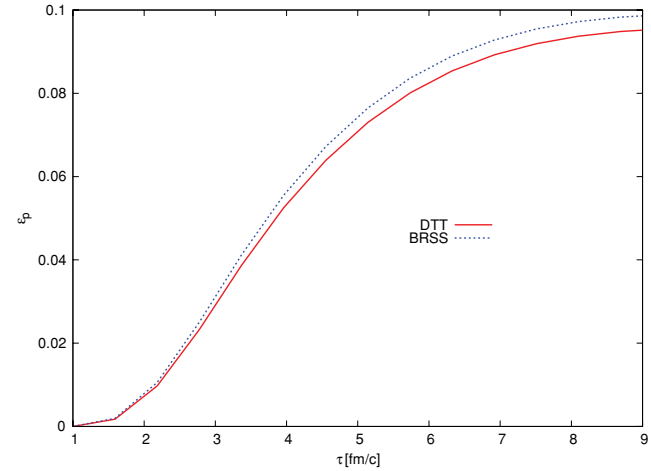

FIG. 3. (Color online) Evolution of the momentum anisotropy for the BRSS and the DTT with $b = 7$ fm, $T_i = 333$ MeV, $T_f = 140$ MeV, and $\eta/s = 0.08$.

It is seen that the spatial anisotropies calculated in the DTT and in the BRSS theory are very similar, and quite independent of η/s. In contrast, the momentum anisotropies are seen to strongly depend on η/s and are very different in the BRSS and the DTT. The DTT ϵ_p is systematically lower that the BRSS one, and, as we will see, this will be reflected on the calculated elliptic flow.

In order to compare the elliptic flow calculated with the DTT or the BRSS theory to data and, in this way, constrain the value of η/s, we will follow the procedure of Luzum and Romatschke in [20]. The idea is to determine the initial temperature T_i for $b = 0$ and T_f by matching the hydrodynamic simulation to total multiplicity and $\langle p_T\rangle$. As explained in Ref. [20], one should refrain from trying to match pion multiplicity and $\langle p_T\rangle$ since the Boltzmann's approximation used in Eq. (16) leads to an unavoidable systematic error. We will therefore aim at a reasonable fit of kaon multiplicity and $\langle p_T\rangle$ to determine T_i and T_f. In

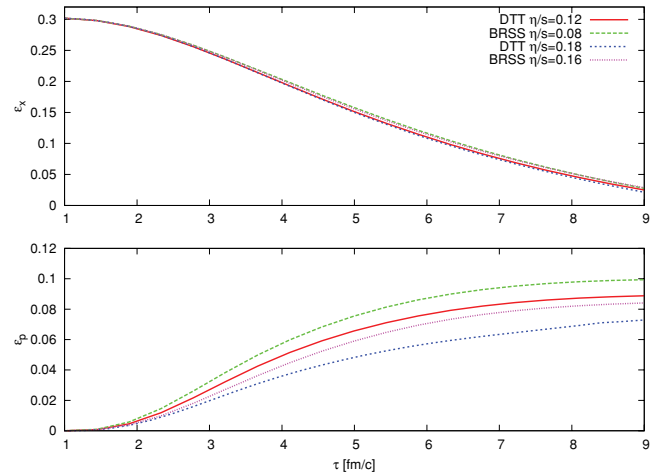

FIG. 4. (Color online) Evolution of the spatial (top) and momentum (bottom) anisotropies for the BRSS model and the DTT with $b = 7$ fm, $T_i = 333$ MeV, $T_f = 140$ MeV, and different values of η/s.

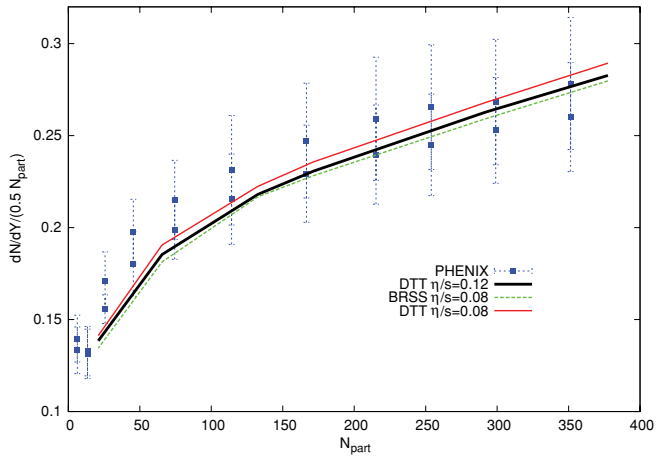

FIG. 5. (Color online) Centrality dependence of total multiplicity for kaon for Au+Au collisions at $\sqrt{s} = 200$ GeV compared to the DTT and the BRSS results for $\eta/s = 0.08$, $T_i = 333$ MeV, and $T_f = 140$ MeV. We also show the DTT result with $\eta/s = 0.12$ and $T_i = 328$ MeV for comparison. Data are from the PHENIX Collaboration [51]. The two sets of data points correspond to K^+ and K^-.

Appendix A we will show that the results for elliptic flow are only weakly dependent on the values of second-order transport coefficients (τ_π, λ_1). For this reason, in the remainder of this section we will use coefficients appropriate for a SYM plasma as given in Eq. (14).

We start by presenting the results for total Kaon multiplicity and $\langle p_T \rangle$ obtained in both models with $\eta/s = 0.08$, $T_i = 333$ MeV, and $T_f = 140$ MeV, compared to PHENIX data [51]. As in the case of spatial and momentum anisotropies, this allows us to evaluate the differences in both hydrodynamic formalisms for the same values of η/s, T_i, and T_f. We also show the results for the DTT with $\eta/s = 0.12$ and $T_i = 328$ MeV (which, as shown later, is the value of T_i that gives, for this value of η/s in the DTT, the best matching to data).

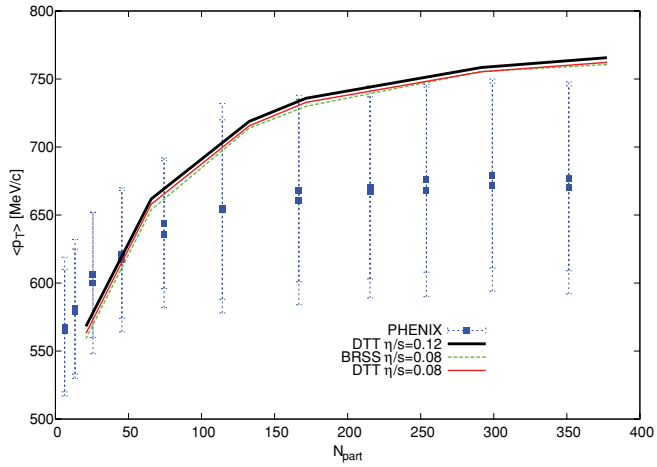

FIG. 6. (Color online) Centrality dependence of $\langle p_T \rangle$ for kaon for Au+Au collisions at $\sqrt{s} = 200$ GeV compared to the DTT and the BRSS results for $\eta/s = 0.08$, $T_i = 333$ MeV, and $T_f = 140$ MeV. We also show the DTT result with $\eta/s = 0.12$ and $T_i = 328$ MeV for comparison. Data are from the PHENIX Collaboration [51].

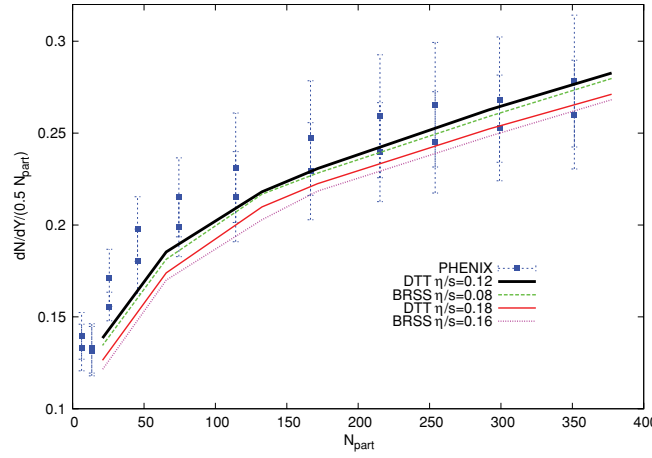

FIG. 7. (Color online) Centrality dependence of total multiplicity for kaon for Au+Au collisions at $\sqrt{s} = 200$ GeV compared to the DTT and the BRSS results for various values of η/s. The freeze-out temperature is $T_f = 140$ MeV. Data are from the PHENIX Collaboration [51].

Figure 5 shows the total multiplicity. The two sets of data points correspond to K^+ and K^-, which cannot be distinguished in our model since the EOS corresponds to zero net-baryon density. It is seen that, in order to achieve the same multiplicity as in the BRSS model, we must take $\eta/s = 0.12$ in the DTT. Figure 6 shows $\langle p_T \rangle$ obtained in both models. It is seen that $\langle p_T \rangle$ is larger in the DTT than in the BRSS, indicating that the DTT leads to larger transverse flow. Larger shear stress leads to larger transverse flow, so the results obtained for $\langle p_T \rangle$ confirm the fact that the DTT leads to stronger dissipation and consequently larger entropy production.

We now proceed to find T_i by matching total kaon multiplicity and $\langle p_T \rangle$ to data. We note that we fix $T_f = 140$ MeV in both models. Figures 7 and 8 show the total multiplicity and $\langle p_T \rangle$ calculated in the BRSS model and the DTT. By performing this combined matching to multiplicity

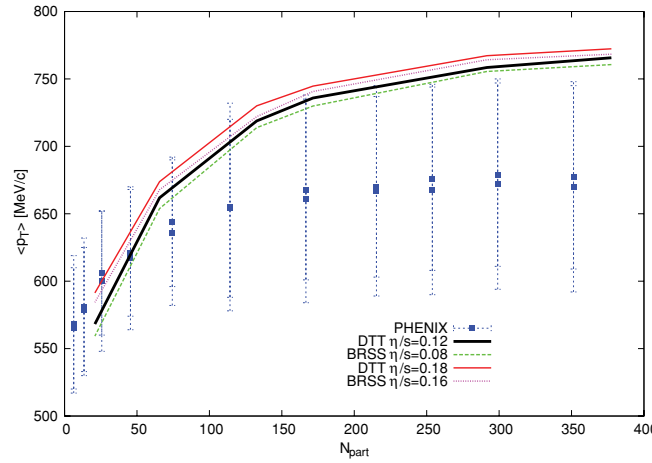

FIG. 8. (Color online) Centrality dependence of $\langle p_T \rangle$ for kaon for Au+Au collisions at $\sqrt{s} = 200$ GeV compared to the DTT and the BRSS results for various values of η/s. The freeze-out temperature is $T_f = 140$ MeV. Data are from PHENIX Collaboration [51].

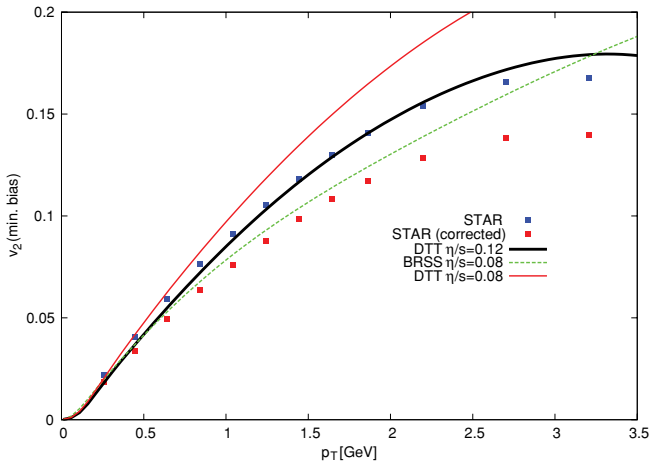

FIG. 9. (Color online) Comparison of STAR data on charged-hadron minimum-bias elliptic flow to DTT and BRSS results with $\eta/s = 0.08$ and $T_i = 333$ MeV. We also show results of the DTT with $\eta/s = 0.12$ and $T_i = 328$ MeV for comparison.

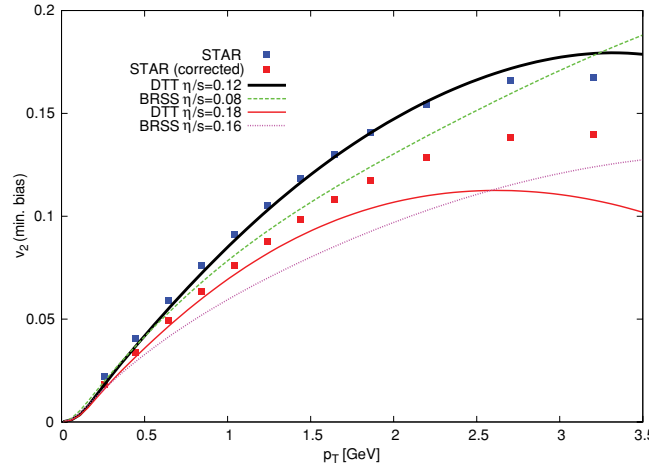

FIG. 10. (Color online) Comparison of DTT results and experimental data on charged-hadron minimum-bias elliptic flow by STAR (event plane) [52]. STAR event-plane data have been reduced by 20% (red squares) to account for nonflow contributions (estimatively) [52]. We also show results for the BRSS model for comparison.

and $\langle p_T \rangle$ data, we find for the DTT that $T_i = 328$ MeV (323 MeV) at $\eta/s = 0.12$ (0.18) gives a reasonable fit to data, comparable to that obtained by the BRSS with $T_i = 333$ MeV (327 MeV) at $\eta/s = 0.08$ (0.16) [20].

With the values for T_i and T_f obtained before, we now calculate the charged-hadron minimum-bias elliptic flow with the DTT and the BRSS and compare the results to data. In Figure 9 we show the elliptic flow calculated in the DTT and the BRSS with $\eta/s = 0.08$ and $T_i = 333$ MeV, and in the DTT with $\eta/s = 0.12$ and $T_i = 328$ MeV, compared to experimental data from the STAR Collaboration [52]. We note that in order to estimate the removal of nonflow contributions to the elliptic flow, we reduce the STAR data by 20% (see Refs. [20,52]). It is seen that using the DTT with $\eta/s = 0.08$ provides a poor fit to data, specially at intermediate and large transverse momentum.

Figure 10 shows the charged-hadron minimum-bias elliptic of the BRSS model and the DTT for different values of η/s, compared to data. The most important differences in the calculated v_2 with the BRSS model and with the DTT take place for $p_T > 2$ GeV. It is seen that v_2 reaches its maximum at lower values of p_T in the DTT, and that the values for η/s for which the DTT model is consistent with data ($\eta/s \leqslant 0.18$) are slightly larger than those for the BRSS. The fact that the values of η/s for which the elliptic flow is consistent with data are the same as those obtained from matching kaon multiplicity and $\langle p_T \rangle$ does not mean that v_2 measurements do not constrain η/s, but rather that viscous hydrodynamics provides a consistent description of these observables in Au+Au collisions.

We now wish to constrain the value of η/s and give an upper bound beyond which our results cease to be consistent with experimental data. From Figs. 5 to 10 we find that we can match the DTT results to experimental data provided $\eta/s \leqslant 0.18$. It is difficult to determine the uncertainty in η/s coming from the hydrodynamic simulation. Considering the dependence of final results on the following factors: (i) the precise value of second-order transport coefficients (see Appendix A), (ii) the mesh grid (see Appendix A), and (iii) the precise value of T_i and T_f obtained from matching hydrodynamic results to data on kaon multiplicity and $\langle p_T \rangle$, as sources of uncertainty in the determination of η/s, we can estimate this theoretical uncertainty as ± 0.07. Taking into account the uncertainty in the removal of nonflow contributions to the measured charged-hadron v_2 (minimum bias) by STAR [52], we can, following Ref. [20], estimate the experimental uncertainty as ± 0.1. Therefore, we conclude that the DTT model favors $\eta/s \leqslant 0.35$. We emphasize that our estimate for η/s does not contemplate the uncertainty coming from several other factors such as bulk viscosity [53,55,56], different temperatures for kinetic and chemical freeze-out [49], precise knowledge of the EOS and of the initial conditions [18,20,21,31], which are expected to have a significant influence on the value of η/s. For this reason, our estimate for η/s should be regarded as a conservative one. One should note, however, that both the DTT and the BRSS are consistent with experimental data, although none of the models can reproduce the saturation of the measured minimum bias elliptic flow. Recent studies [54–57] suggest that the origin of this failure of viscous hydrodynamics to reproduce saturation of the elliptic flow is Grad's quadratic ansatz for the nonequilibrium correction to the thermal distribution function given by Eq. (16).

Finally, we note that this result for η/s is in good agreement with the upper bound found in several other works [3,20,21] by similar matching of viscous hydrodynamics to data, and supports the notion that the matter created at RHIC exhibits almost perfect fluidity.

IV. SUMMARY AND CONCLUSIONS

We have studied the space-time evolution of a conformal plasma in $2 + 1$ dimensions using second-order as well as divergence-type dissipative hydrodynamics. In the simulations, we employed a simple Glauber model to calculate the initial energy-density distribution, a model equation of state with an analytic crossover, and the Cooper-Frye prescription

for isothermal freeze-out (the latter implemented in the code UVH2+1 [20,32]).

We have made a comparison of the calculated kaon total multiplicity and $\langle p_T \rangle$ with experimental data by the PHENIX Collaboration [51], as well as of the elliptic flow with experimental data by the STAR Collaboration [52]. We have found that the difference between the BRSS and the DTT elliptic flows starts to become significant when $p_T > 2$ GeV; the elliptic flow calculated with the DTT reaches its maximum at lower values of p_T. Including an estimate for the uncertainty in the determination of η/s from data, we find that the DTT can be matched to RHIC data provided $\eta/s \leqslant 0.35$, in good agreement with previous studies based on Israel-Stewart or BRSS equations. The results we obtain also show that the differences between hydrodynamic formalisms are a significant source of uncertainty in the precise extraction of η/s from data.

We note that neither the DTT nor the BRSS model is able to reproduce the experimental saturation of elliptic flow at $p_T \gtrsim 2.5$ GeV, possibly pointing to the incorrectness of Grad's ansatz for the nonequilibrium distribution function [Eq. (16)]. A related aspect that surely deserves further investigation is the inclusion of bulk viscosity in the hadronic stage of the fireball's evolution and during the deconfinement crossover. In this respect, it should be noted that recent work [55] has raised concern about the validity of Grad's ansatz for a reliable computation of freeze-out when bulk viscosity is present (see also Ref. [56] for a different treatment of bulk viscosity). It was found in Ref. [55] that the nonequilibrium corrections due to bulk viscosity to the distribution function are considerably larger than those coming from shear viscosity, rendering the application of Grad's moment method doubtful when bulk viscosity is taken into account. Moreover, Luzum and Ollitrault [54] have found that even for a conformal plasma Grad's ansatz is disfavored by data on $v_4/(v_2)^2$, while Dusling, Moore, and Teaney [57] have calculated the momentum dependence of the nonequilibrium contribution to the distribution function in a weak coupling setting and found it proportional to $p_T^{3/2}$.

It would therefore be interesting to study this point within the framework of DTTs. In order to further investigate this issue, the relation between the DTT and microscopic theory must be precisely determined.

ACKNOWLEDGMENTS

We are grateful to Paul Romatschke, Tomoi Koide, and Akihiko Monnai for useful comments and interesting discussions. We thank Roy Lacey for bringing Ref. [2] to our attention, and A. Poskanzer for providing data from the STAR Collaboration. This work has been supported in part by ANPCyT, CONICET, and UBA (Argentina).

APPENDIX A: DEPENDENCE ON TRANSPORT COEFFICIENTS AND GRID

In this appendix we will evaluate the dependence of the results obtained with the DTT on the spatial mesh and on the values for second-order transport coefficients. The parameters used for this evaluation are $\eta/s = 0.08$, $\tau_0 = 1$ fm/c, $T_i = 333$ MeV, and $T_f = 140$ MeV in both cases.

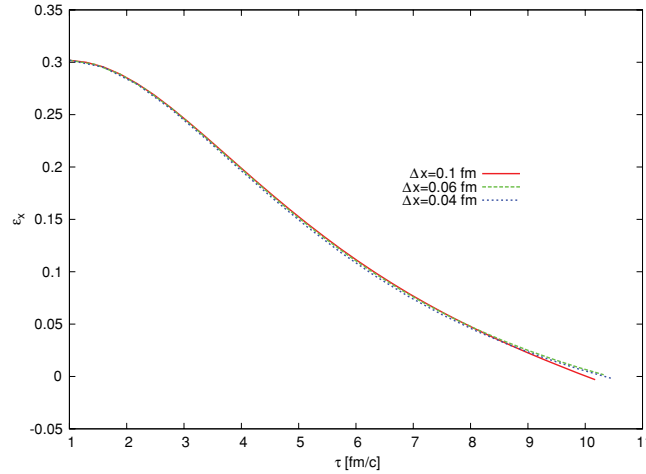

FIG. 11. (Color online) Evolution of the spatial anisotropy in the DTT with $\eta/s = 0.08$ and $b = 7$ fm for different values of the space grid Δx.

In Fig. 11 we show the evolution of spatial anisotropy ϵ_x for a collision with $b = 7$ fm and a time step $\Delta\tau = 0.002$ fm/c for different values of the space grid $\Delta x = 0.1$, 0.06, and 0.04 fm. It is seen that the dependence of ϵ_x on Δx is very small and only significant at late times. There is practically no difference between the results obtained with $\Delta x = 0.06$ fm and 0.04 fm, and, for this reason, we employ $\Delta x = 0.06$ fm in all the simulations shown in this work. We have also checked that diminishing the time step did not change the results appreciably, and therefore use $\Delta\tau = 0.002$ fm/c throughout.

A convenient quantity to measure the influence of second-order coefficients on final hadron observables is the elliptic flow coefficient $\tilde{v}_2$ [see Eq. (18)]. In Fig. 12 we show the

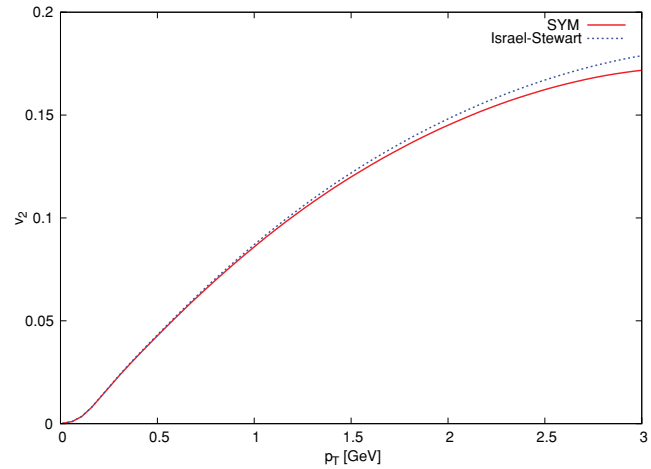

FIG. 12. (Color online) Charged-hadron elliptic flow calculated in the DTT with $\eta/s = 0.08$ and $b = 7$ fm with $\tau_\pi = 2(2 - \ln 2)\eta/sT$ and $\lambda_1 = \eta/2\pi T$, corresponding to a SYM plasma, and with $\tau_\pi = 6\eta/sT$ and $\lambda_1 = 0$, corresponding to weakly coupled Israel-Stewart theory.

charged-hadron elliptic flow calculated in the DTT with $\eta/s = 0.08$ and $b = 7$ fm for two sets of second-order coefficients, namely, those of a SYM plasma given in Eq. (14) and those corresponding to weakly coupled Israel-Stewart formalism ($\tau_\pi = 6\eta/sT$ and $\lambda_1 = 0$). It is seen that the difference between v_2 calculated with both sets of coefficients is negligible for $p_T < 1.5$ GeV and small for higher p_T. It is interesting to note that, although both curves are very similar, the elliptic flow calculated for the SYM plasma reaches its maximum at a lower value of p_T. We conclude that the results depend only weakly on the precise values of τ_π and λ_1, at least for low values of η/s. This is in agreement with the findings of Ref. [20].

APPENDIX B: DIVERGENCE-TYPE THEORIES

In this appendix we give a brief summary of DTTs. Detailed discussions can be found in Refs. [26,28,29].

According to Geroch and Lindblom [26], the hydrodynamical description of a nonequilibrium state requires, besides the particle current N_μ and the stress-energy tensor $T_{\mu\nu}$, a new third-order tensor $A_{\mu\nu\rho}$ obeying an equation of motion of divergence type. The dynamical equations are the conservation laws of N_μ and $T_{\mu\nu}$, together with an equation describing the dissipative part,

$$D_\mu A^{\mu\nu\rho} = I^{\nu\rho}, \tag{B1}$$

where $A^{\mu\nu\rho}$ and $I^{\nu\rho}$ are algebraic local functions of N^μ and $T^{\mu\nu}$ and symmetric in the indices (ν, ρ), and D_μ is the covariant derivative. The entropy current is extended to

$$S^\mu = \Phi^\mu - \beta_\nu T^{\mu\nu} - \alpha N^\mu - A^{\mu\nu\rho}\xi_{\nu\rho}, \tag{B2}$$

where $\beta_\nu = u_\nu/T$ is the temperature vector, $\alpha = \mu/T$ is the affinity, Φ^μ is the thermodynamic potential, and $\xi_{\nu\rho}$ is symmetric and traceless and vanishes in equilibrium.

We now require that the entropy and the thermodynamical potential be algebraic functions of $(\alpha, \beta_\mu, \xi_{\mu\nu})$. If the entropy production is to be nonnegative, then

$$\frac{\partial\Phi^\mu}{\partial\alpha} = N^\mu; \quad \frac{\partial\Phi^\mu}{\partial\beta_\nu} = T^{\mu\nu}; \quad \frac{\partial\Phi^\mu}{\partial\xi_{\nu\rho}} = A^{\mu\nu\rho}. \tag{B3}$$

Thus, as a consequence of the equations of motion, the entropy production rate is

$$D_\mu S^\mu = -I^{\nu\rho}\xi_{\nu\rho}. \tag{B4}$$

Since the stress-energy tensor is symmetric, we must also have

$$\Phi^\mu = \frac{\partial\chi}{\partial\beta_\mu}, \tag{B5}$$

where $\chi(\alpha, \beta_\mu, \xi_{\mu\nu})$ is the so-called generating function of the theory. This means that every DTT is completely determined once χ and I are specified as algebraic functions of $\alpha, \beta_\mu, \xi_{\mu\nu}$. The theory thus constructed satisfies the principles of relativity and entropy, and fully exploits the latter [28].

Introducing the symbols ζ^A to denote the set $(\alpha, \beta_\mu, \xi_{\mu\nu})$, A^μ_B the set $(N^\mu, T^{\mu\nu}, A^{\mu\nu\rho})$, and I_B the set $(0, 0, I_{\mu\nu})$, the theory is summed up in the following equations:

$$\begin{aligned} A^\mu_B &= \frac{\partial\Phi^\mu}{\partial\zeta^B}, \\ D_\mu S^\mu &= -I_B\zeta^B, \\ D_\mu A^\mu_B &= I_B. \end{aligned} \tag{B6}$$

We will now review the main results of Ref. [25] where a quadratic DTT for a conformal fluid in $d = 4$ dimensions was developed. The most general generating function χ that is quadratic in $\xi^{\mu\nu}$ is

$$\begin{aligned} \chi &= \chi_0(T) + \chi_1(T)\xi_{\mu\nu}u^\mu u^\nu \\ &\quad + \frac{1}{2T^\alpha}(Au_\rho\xi^{\rho\sigma}\xi_{\sigma\tau}u^\tau + B\xi^{\rho\sigma}\xi_{\rho\sigma}), \end{aligned} \tag{B7}$$

where (α, A, B) are coefficients to be determined.

For a conformal field, $T^{\mu\nu} \to e^{6\omega(x^\gamma)}T^{\mu\nu}$ under a Weyl transformation $g_{\mu\nu} \to e^{-2\omega(x^\gamma)}g_{\mu\nu}$ and $g_{\mu\nu}T^{\mu\nu} = 0$. These constraints pose no problem for $\chi_0(T)$ and $\chi_1(T)$ and, in combination with the second equation of (B3), lead to

$$\chi_0(T) = \frac{a}{6}T^2, \quad \chi_1(T) = \frac{\eta}{2}T^{-2}, \tag{B8}$$

where the energy density is $\rho = aT^4$.

For the quadratic part of χ, it is necessary to redefine the temperature in order to satisfy both constraints. To ensure that $T^{\mu\nu}$ has the correct conformal weight we need $\alpha = 6$. The quadratic stress-energy tensor obtained from χ then reads

$$T^{\mu\nu}_2 = \tfrac{1}{2}T^{-4}\big[B(30u^\mu u^\nu - 6\Delta^{\mu\nu})\xi^{\rho\sigma}\xi_{\rho\sigma} + 2A\xi^{\mu\rho}\xi^\nu_\rho\big]. \tag{B9}$$

To get $T^\mu_{2,\mu} = 0$ we need $A = 24B$. The idea is to put

$$T^{\mu\nu}_2 = \Pi^{\mu\nu} + \delta T^{\mu\nu}_2, \tag{B10}$$

with $\Pi^{\mu\nu}$ traceless and transverse, and $\delta T^{\mu\nu}_2$ traceless. We get

$$\Pi^{\mu\nu}_2 = AT^{-4}\left[\xi^{\mu\rho}\xi^\nu_\rho - \tfrac{1}{3}\Delta^{\mu\nu}\xi^{\rho\sigma}\xi_{\rho\sigma}\right] \tag{B11}$$

and

$$\delta T^{\mu\nu}_2 = \tfrac{5}{8}T^{-4}A\left(u^\mu u^\nu + \tfrac{1}{3}\Delta^{\mu\nu}\right)\xi^{\rho\sigma}\xi_{\rho\sigma}. \tag{B12}$$

Defining the physical temperature T_p by $2T^4 = T_p^4 + \sqrt{T_p^8 - (5A/2a)\xi^{\rho\sigma}\xi_{\rho\sigma}}$ we obtain

$$T^{\mu\nu} = \rho_p u^\mu u^\nu + p_p\Delta^{\mu\nu} + \Pi^{\mu\nu} \tag{B13}$$

with

$$\Pi^{\mu\nu} = \eta\xi^{\mu\nu} + AT^{-4}\left(\xi^{\mu\alpha}\xi^\nu_\alpha - \tfrac{1}{3}\Delta^{\mu\nu}\xi^{\alpha\gamma}\xi_{\alpha\gamma}\right) \tag{B14}$$

and $\rho_p = aT_p^4$.

The source term is written as $I^{\mu\nu} = I^{\mu\nu}_1 + I^{\mu\nu}_2$, where $I^{\mu\nu}_{1,2}$ are linear and quadratic in $\xi^{\rho\sigma}$, respectively. $I^{\mu\nu}_1$ is obtained by requiring the DTT to reproduce Eckart's theory at first order in velocity gradients, while $I^{\mu\nu}_2$ is obtained by requiring that the quadratic DTT satisfy the second law exactly. The result is

$$I^{\mu\nu} = -\frac{\eta}{2T}\xi_{\mu\nu} + gT^{-8}\Delta^{\mu\nu}\xi_{\rho\sigma}\xi^{\rho\sigma}, \tag{B15}$$

whereby the entropy production reads

$$D_\mu S^\mu = \frac{\eta}{2T}\xi_{\rho\sigma}\xi^{\rho\sigma}. \tag{B16}$$

By requiring the DTT to reproduce the BRSS when $\xi^{\mu\nu}$ is expanded at second order in velocity gradients, the relation between (A, g) and (τ_π, λ_1) is found to be

$$A = -\frac{\lambda_1\tau_\pi}{3\eta}T^8 \tag{B17}$$

and

$$g = -\frac{\lambda_1 T^7}{9}. \tag{B18}$$

The equation of motion for the third-order tensor $D_\mu A^{\mu\nu\rho} = I^{\nu\rho}$ renders an evolution equation for $\xi^{\nu\rho}$. In $2+1$ the evolution is given by Eq. (8). We note that in Ref. [25] we have set $T = T_p$ since the extra terms arising when using T_p are of higher order (i.e., are terms that would be obtained from a cubic generating function χ). We have numerically checked that these extra terms are negligible; thus one can use $T = T_p$ without appreciable change in the results.

[1] K. Adcox *et al.* (PHENIX Collaboration), Nucl. Phys. A **757**, 184 (2005).

[2] R. A. Lacey, N. N. Ajitanand, J. M. Alexander, P. Chung, W. G. Holzmann, M. Issah, A. Taranenko, P. Danielewicz, and Horst Stocker, Phys. Rev. Lett. **98**, 092301 (2007); R. A. Lacey, N. N. Ajitanand, J. M. Alexander, X. Gong, J. Jia, A. Taranenko, and Rui Wei, Phys. Rev. C **80**, 051901 (2009); R. A. Lacey, A. Taranenko, and R. Wei, arXiv:0905.4368 [nucl-exp].

[3] S. Gavin and M. Abdel-Aziz, Phys. Rev. Lett. **97**, 162302 (2006); H. J. Drescher, A. Dumitru, C. Gombeaud, and J. Y. Ollitrault, Phys. Rev. C **76**, 024905 (2007); A. K. Chaudhuri, Phys. Lett. B **681**, 418 (2009).

[4] D. H. Rischke, in *Proceedings of the 11th Chris Engelbrecht Summer School in Theoretical Physics: Hadrons in Dense Matter and Hadrosynthesis*, *Cape Town, South Africa*, *1998*, edited by J. Cleymans, H. B. Geyer, and F. G. Scholtz, Lecture Notes in Physics Vol. 516 (Springer-Verlag, Germany, 1999).

[5] U. W. Heinz, arXiv:0901.4355 [nucl-th].

[6] P. Romatschke, Int. J. Mod. Phys. E **19**, 1 (2010).

[7] A. El, A. Muronga, Z. Xu, and C. Greiner, Phys. Rev. C **79**, 044914 (2009); A. Muronga, *ibid.* **69**, 034903 (2004).

[8] P. Huovinen and D. Molnar, Phys. Rev. C **79**, 014906 (2009).

[9] U. Heinz, H. Song, and A. K. Chaudhuri, Phys. Rev. C **73**, 034904 (2006).

[10] P. K. Kovtun, D. T. Son, and A. O. Starinets, Phys. Rev. Lett. **94**, 111601 (2005); E. Shuryak, Prog. Part. Nucl. Phys. **62**, 48 (2009); M. P. Heller, R. A. Janik, and R. Peschanski, Acta Phys. Pol. **39**, 3183 (2008); D. T. Son and A. O. Starinets, Annu. Rev. Nucl. Part. Sci. **57**, 95 (2007); M. Rangamani, Class. Quant. Grav. **26**, 224003 (2009).

[11] A. K. Chaudhuri, arXiv:0704.0134 [nucl-th].

[12] D. Teaney, Nucl. Phys. A **830**, 891 (2009).

[13] P. Sorensen, in *Quark-Gluon Plasma*, Vol. 4, edited by R. C. Hwa and X. Wang (World Scientific, Singapore, 2010).

[14] E. Shuryak, Prog. Part. Nucl. Phys. **62**, 48 (2009).

[15] E. Calzetta and B.-L. Hu, *Nonequilibrium Quantum Field Theory* (Cambridge University Press, Cambridge, 2008).

[16] D. Teaney, J. Lauret, and E. V. Shuryak, Phys. Rev. Lett. **86**, 4783 (2001); P. Huovinen, P. F. Kolb, U. W. Heinz, P. V. Ruuskanen, and S. A. Voloshin, Phys. Lett. B **503**, 58 (2001); T. Hirano and K. Tsuda, Phys. Rev. C **66**, 054905 (2002); P. F. Kolb and R. Rapp, *ibid.* **67**, 044903 (2003); Piotr Bozek and Iwona Wyskiel, *ibid.* **79**, 044916 (2009).

[17] B. I. Abelev *et al.* (STAR Collaboration), Phys. Rev. C **81**, 044902 (2010).

[18] P. Huovinen and P. Petreczky, Nucl. Phys. A **837**, 26 (2010); P. Huovinen, *ibid.* **761**, 296 (2005); T. Hirano and M. Gyulassy, *ibid.* **769**, 71 (2006); U. W. Heinz, J. Phys. G **31**, S717 (2005); P. Huovinen, Eur. Phys. J. A **37**, 121 (2008).

[19] H. Song, Ph.D. thesis, Ohio State University, 2009.

[20] M. Luzum and P. Romatschke, Phys. Rev. C **78**, 034915 (2008); **79**, 039903(E) (2009).

[21] M. Luzum, Ph.D. thesis, University of Washington, 2009.

[22] W. Israel, Ann. Phys. (NY) **100**, 310 (1976); W. Israel and J. Stewart, *ibid.* **118**, 341 (1979).

[23] I. Bouras, E. Molnar, H. Niemi, Z. Xu, A. El, O. Fochler, C. Greiner, and D. H. Rischke, arXiv:1006.0387 [hep-ph]; Nucl. Phys. A **830**, 741 (2009).

[24] D. Jou and D. Pavon, Phys. Rev. A **44**, 6496 (1991).

[25] J. Peralta-Ramos and E. Calzetta, Phys. Rev. D **80**, 126002 (2009).

[26] R. Geroch and L. Lindblom, Phys. Rev. D **41**, 1855 (1990).

[27] R. Geroch and L. Lindblom, Ann. Phys. (NY) **207**, 394 (1991).

[28] I.-S. Liu, I. Muller, and T. Ruggeri, Ann. Phys. (NY) **169**, 191 (1986); T. Ruggeri, in *Relativistic Fluid Dynamics*, Lecture Notes in Mathematics, Vol. 1385, edited by A. Anile and Y. Choquet-Bruhat (Springer-Verlag, Germany, 1989).

[29] E. Calzetta, Class. Quant. Grav. **15**, 653 (1998).

[30] K. Dusling and D. Teaney, Phys. Rev. C **77**, 034905 (2008).

[31] H. Song and U. Heinz, Phys. Rev. C **77**, 064901 (2008).

[32] P. Romatschke and U. Romatschke, Phys. Rev. Lett. **99**, 172301 (2007).

[33] T. Koide, G. S. Denicol, Ph. Mota, and T. Kodama, Phys. Rev. C **75**, 034909 (2007).

[34] A. El, Z. Xu, and C. Greiner, Phys. Rev. C **81**, 041901 (2010).

[35] M. Lublinsky and E. Shuryak, Phys. Rev. D **80**, 065026 (2009).

[36] R. Baier, P. Romatschke, D. T. Son, A. O. Starinets, and M. A. Stephanov, J. High Energy Phys. 04 (2008) 100.

[37] S. Bhattacharyya, V. E. Hubeny, S. Minwalla, and M. Rangamani, J. High Energy Phys. 02 (2008) 045.

[38] M. Natsuume and T. Okamura, Phys. Rev. D **77**, 066014 (2008); **78**, 089902(E) (2008).

[39] R. Baier, P. Romatschke, and U. A. Wiedemann, Phys. Rev. C **73**, 064903 (2006); B. Betz, D. Henkel, and D. H. Rischke, J. Phys. G **36**, 064029 (2009); M. A. York and G. D. Moore, Phys. Rev. D **79**, 054011 (2009); A. Muronga, Phys. Rev. C **76**, 014910 (2007).

[40] M. Panero, Phys. Rev. Lett. **103**, 232001 (2009).

[41] R. Baier and P. Romatschke, Eur. Phys. J. C **51**, 677 (2007).
[42] P. F. Kolb, U. W. Heinz, P. Huovinen, K. J. Eskola, and K. Tuominen, Nucl. Phys. A **696**, 197 (2001).
[43] M. Laine and Y. Schröder, Phys. Rev. D **73**, 085009 (2006).
[44] Y. Aoki, G. Endrodi, Z. Fodor, S. D. Katz, and K. K. Szabo, Nature (London) **443**, 675 (2006).
[45] F. Cooper and G. Frye, Phys. Rev. D **10**, 186 (1974).
[46] S. R. de Groot, W. A. van Leeuwen, and Ch. G. van Weert, *Relativistic Kinetic Theory* (North-Holland, Amsterdam, 1980); J. M. Stewart, *Non-Equilibrium Relativistic Kinetic Theory*, Lecture Notes in Physics Vol. 10 (Springer, Berlin, 1971).
[47] J. Sollfrank, P. Koch, and U. W. Heinz, Z. Phys. C **52**, 593 (1991); Phys. Lett. B **252**, 256 (1990).
[48] P. F. Kolb, J. Sollfrank, and U. Heinz, Phys. Rev. C **62**, 054909 (2000); P. F. Kolb and R. Rapp, *ibid.* **67**, 044903 (2003); P. F. Kolb and U. Heinz, arXiv:nucl-th/0305084. AZHYDRO code v0.2 is available from [http://karman.physics.purdue.edu/OSCAR].
[49] U. W. Heinz and G. Kestin, Eur. Phys. J. ST **155**, 75 (2008).
[50] A. K. Chaudhuri, Phys. Rev. C **74**, 044904 (2006).
[51] S. S. Adler *et al.* (PHENIX Collaboration), Phys. Rev. C **69**, 034909 (2004).
[52] B. I. Abelev *et al.* (STAR Collaboration), Phys. Rev. C **77**, 054901 (2008).
[53] G. S. Denicol, T. Kodama, and T. Koide, arXiv:1002.2394 [nucl-th]; P. Bozek, Phys. Rev. C **81**, 034909 (2010); H. Song and U. W. Heinz, Phys. Rev. C **81**, 024905 (2010); A. Monnai and T. Hirano, Nucl. Phys. A **830**, 471 (2009).
[54] M. Luzum and J.-Y. Ollitrault, Phys. Rev. C **82**, 014906 (2010).
[55] G. S. Denicol, T. Kodama, T. Koide, and Ph. Mota, Phys. Rev. C **80**, 064901 (2009).
[56] A. Monnai and T. Hirano, Phys. Rev. C **80**, 054906 (2009).
[57] K. Dusling, G. Moore, and D. Teaney, Phys. Rev. C **81**, 034907 (2010).